Damage detection using stress and ultrasonic waves

Wieslaw Staszewski, Christian Boller, Sébastien Grondel, C. Biemans, E. O'Brien, Christophe Delebarre, G. R. Tomlinson

Damage Detection Using Stress and Ultrasonic Waves

W.J. Staszewski[1], C. Boller1, S. Grondel[2],C.Biemans[3], E. O'Brien4, C.Delebarre[2] and G.R. Tomlinson[1]

1 Department of Mechanical Engineering, Sheffield University, Sheffield, UK
2 IEMN, Valenciennes, France
3 DaimlerChrysler, Berlin, Germany
4 Airbus UK, Filton, UK

4.1 INTRODUCTION

Elastic waves and their propagation have been used for many years to analyse impact response problems, mechanical properties of various materials and structural damage. Various types of methods based on sound and ultrasound are applied for nondestructive testing (NDT). Acoustic Emission and Ultrasonic inspection are the most widely used techniques in industrial applications. The first technique is passive and does not require any external signal excitation; stress waves are structure-born and produced internally by defects. The second approach requires high-frequency external excitation. The maturity and proven damage detection applications are the major advantages of these techniques. The Acousto-Ultrasonic approach combines elements of Acoustic Emission and Ultrasonic inspection. Although the method has been around for more than thirty years, it has not been used widely in practice. Recent advancements in this area include applications of guided ultrasonic waves. Lamb waves are particularly attractive for damage detection in aerospace structures; a vast amount of literature has been published over the last ten years.

This chapter briefly discusses damage detection methods based on sound and ultrasound. Various elements related to wave propagation mechanism, monitoring strategy and

transducer schemes are discussed. The focus is on definitions, basic principles, similarities and dissimilarities between different techniques. For more details the reader is referred to the appropriate literature. Engineering applications are illustrated using damage detection case studies. Further application examples of Acoustic Emission and Lamb wave based damage detection are given in Chapter 6.

4.2 ACOUSTIC EMISSION

4.2.1 Background

Acoustic Emission (AE) is one of the first and most widely used NDT techniques for structural damage detection. This is supported by a number of literature references related to the subject (e.g. (Scott 1991; Muravin 2000; Holroyd 2001)). The technique relies on transient sound waves propagating in the analysed material. Most of these waves are short-time transient events (burst signals) of significant energy between 100–1000 kHz. The waves can propagate long distances in circles, i.e. in all possible directions (Figure 4.1). Therefore AE testing can cover large, often inaccessible, monitored areas. The distance of propagation depends on material properties, geometry, frequency and environment.

Acoustic events at their origin are high-frequency (in MHz), wideband impacts emitted internally by microcracks and/or inclusion de-cohesion (e.g. metallic inclusions, bubbles) under external loading applied to monitored specimens. These material defects release elastic energy due to rapid local stress redistribution as a result of loading. The energy results from growing cracks, rubbed surfaces of cracks or dislocations. Other sources of AE are also possible such as phase transformation or melting. The AE process is similar to seismic waves propagating as a result of dislocations of various rock formations leading to earthquakes. In contrast to other sound/ultrasound-based techniques it is a passive as well as static method of damage detection, when using the terms mentioned in Chapter 1 before; AE transducers listen to the monitored structure. A relatively small number of sensors is required to cover large monitored areas.

4.2.2 Transducers

AE waves propagating in the monitored specimen can be detected by appropriate transducers which convert mechanical energy into electrical signals. There exist various types

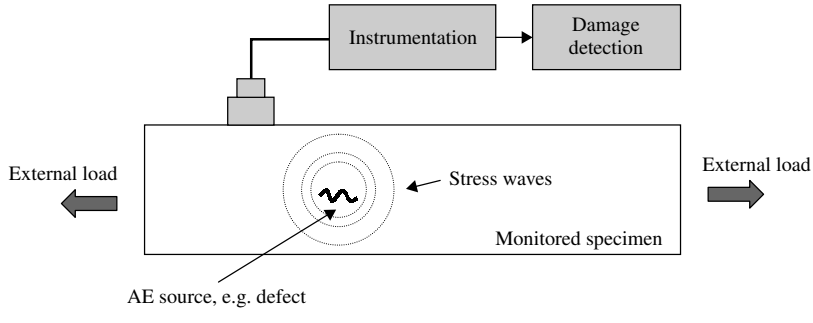

Figure 4.1 Acoustic Emission principle

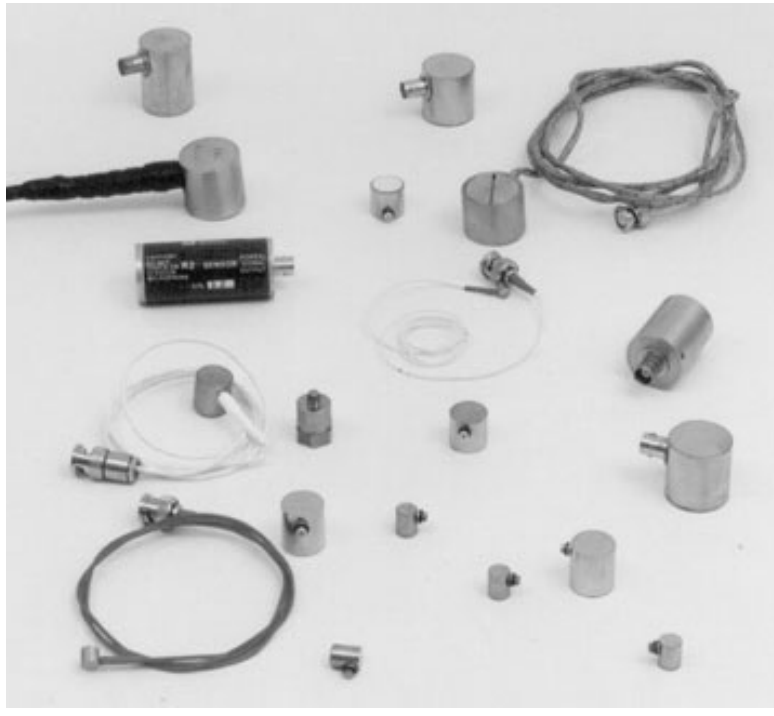

Figure 4.2 Acoustic Emission transducers (reproduced by the permission of MISTRAS Holdings Corp.)

of AE transducers such as piezoelectric, electrodynamic, laser and capacitance sensors. Piezoelectric transducers are well-proven and by far the most widely used for AE testing. Figure 4.2 shows examples of classical piezoelectric transducers. The sensitivity of AE transducers is determined by the bandwidth and the resonance frequency. The sensitivity in general is defined using a logarithmic scale given in dB as

$$A = 20 \times \log \frac{U}{U_{ref}} \tag{4.1}$$

where U is the output voltage from the sensor and U_{ref} is the reference voltage equal to $1\,\mu$V. Sensors data need to be amplified before further signal processing. Often pre-amplifiers are integrated with some types of sensors. Sensors are usually mounted using magnetic holding devices, clamps or glue. Good acoustic contact between the sensor and the monitored surface is essential for AE testing. When the sensor is not permanently bonded on the surface, often special types of coupling agents (e.g. silicon grease, oil) are required.

4.2.3 Signal Processing

There are two types of AE signals encountered in practice: these are transient (or burst); and continuous signals. Transient signals can be separated in time, i.e. the beginning and

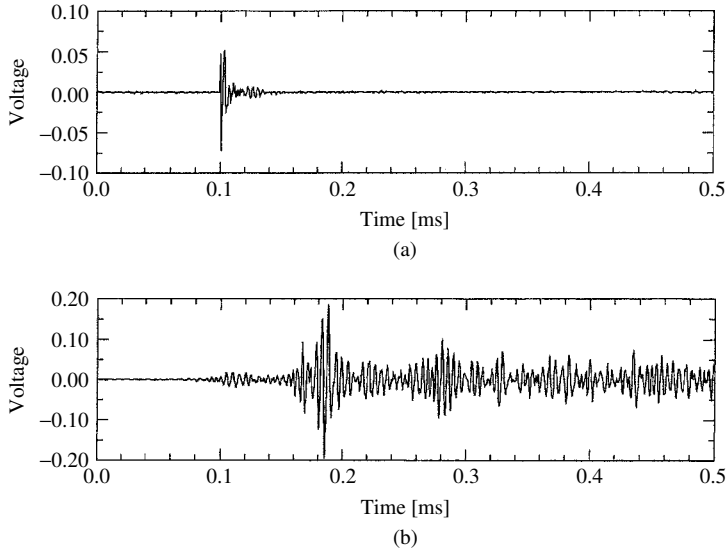

Figure 4.3 Acoustic Emission burst (a) and continuous; (b) signals (Staszewski and Holford 2001)

end of these signals can be identified. They result from acoustic events due to local defects. Continuous signals cannot be separated in time. They are produced by various unwanted phenomena, e.g. plastic deformation or friction. These signals often include background noise which can include both mechanical and electrical disturbances. Figure 4.3 gives examples of burst and continuous AE signals.

Various signal processing techniques are used to analyse AE signals and extract features related to defects. Usually, a threshold level is defined. The AE threshold needs to be exceeded before further analysis. A number of well-defined standard parameters are then used in order to identify defects. This includes:

- Peak amplitude – maximum amplitude of the signal;
- Arrival time – absolute time when the signal first crosses the threshold level;
- Duration time – time interval between the first and last crossings of the threshold;
- Rise time – time interval between the first threshold crossing and the peak amplitude;
- Ring down count – number of threshold level crossings.

Figure 4.4 summarises AE parameter used for damage detection. Often the amplitude values of the AE signal are integrated over the duration time in order to estimate the energy of the burst signal. The level of the background noise can be estimated calculating the Root Mean Square (RMS) value of the signal before the arrival time. Various clustering techniques of AE signals are used in order to mark and locate the highest AE activities. The information obtained from AE tests is displayed using numerical (cumulative or differential characteristics giving total number of events, total energy or pressure) and/or graphical (cluster graphs giving source location) diagrams. Signal waveforms can also be analysed using the time and frequency domains. Source location is possible using arrays

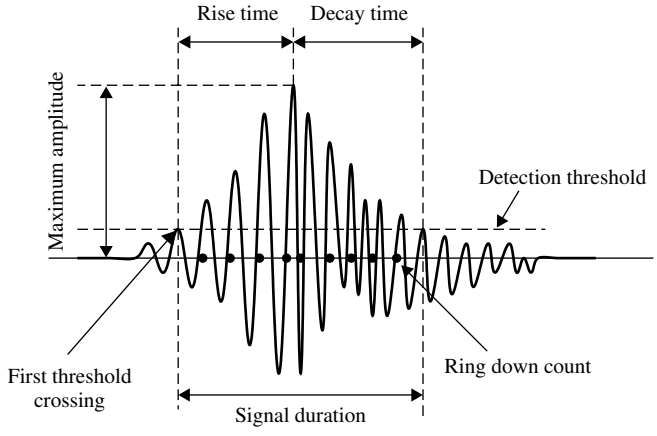

Figure 4.4 Summary of Acoustic Emission parameters used for damage detection

of sensors. Once the sound velocity and signal arrival time differences to these sensors are known, damage location can be estimated using classical triangulation procedures.

4.2.4 Testing and Calibration

AE testing comprises three major steps: detection of AE activities (damage detection), estimation of the AE burst rate (damage severity) and AE source location (damage location). All steps require the AE equipment to be calibrated. This involves an electronic waveform generator (often called a pulser) which produces pre-defined transient signal or a special device which simulates an AE event using the break of the pencil graphite lead. The later device is commonly known as the Hsu–Nielsen source, after the developers of the technique. The break of a 2H 0.5 mm diameter pencil lead approximately 3 mm from its tip generates an acoustic signal which is similar to a natural AE burst.

AE detects damage in the moment of its occurrence. Defect characteristics are unique events and once the event is missed signals cannot be reproduced. Therefore successful damage detection often requires continuous monitoring in service. Also, defects (e.g. cracks) that do not grow are not detected. Burst signals depend on loading and environmental conditions. It is important to monitor these effects for the reference.

The AE testing offers relatively rapid inspection for damage and what is important it can be used for a wide variety of materials. The method offers global monitoring and does not require access to whole monitored areas.

4.3 ULTRASONICS

4.3.1 Background

There exist various damage detection techniques based on ultrasound (Buirks *et al*. 1991; Rose 1999; Schmerr 1998). Classical ultrasonic techniques utilise various phenomena

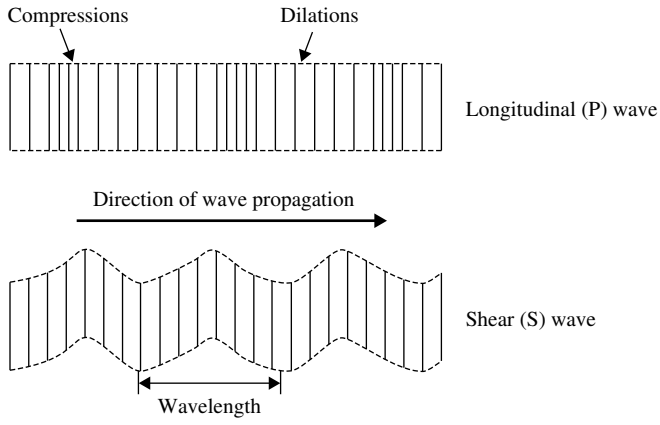

Figure 4.5 Longitudinal (a) and shear (b) bulk waves

and/or properties of ultrasonic waves propagating in the material in order to detect defects. It is well known that various types of waves can propagate in solids. Longitudinal (often called compressional, dilatational pressure or P-wave) and shear (often called transverse or S-wave) waves are the most commonly used wave modes for ultrasonic testing. Both types of waves are represented graphically in Figure 4.5. The direction of particle motion is either in the direction (longitudinal waves) or perpendicular (shear waves) to the direction of wave propagation.

The velocity of propagating waves is one of the most important parameters in ultrasonics. The relationship between the velocity of the longitudinal ultrasonic wave and elastic properties of the material is often used to evaluate the condition of the structure. This relationship can be given as

$$v^2 \approx \frac{E_L}{\rho} \tag{4.2}$$

where v is the velocity of the longitudinal ultrasonic wave, E_L is the longitudinal modulus of elasticity and ρ is the density of the monitored specimen. Similarly, the square velocity of the shear wave is proportional to the shear modulus E_s over density.

Ultrasonic waves can travel long distances in solid materials. However, the energy of sound decreases with the distance of propagation. Propagating waves are additionally scattered (or reflected) and absorbed by different material/structural boundaries. As a result, the amplitude of propagating waves is attenuated. When a wave passes between different media, the velocity of propagation changes. Additionally, various mode conversions can occur. Ultrasonic testing utilises wave attenuation, reflection and refraction for damage detection. Successful NDT requires an understanding of the ultrasonic field. This involves not only wave propagation principles but also problems related to pressure variations, directivity analysis and beam angle of divergence, as discussed in (Rose 1999).

It is important for successful damage detection that the wavelength of ultrasound used for testing is of the order of the defect's size. The wavelength λ can be calculated as

$$\lambda = \frac{c}{f} \tag{4.3}$$

where c is the wave velocity and f is the input frequency. This formula is valid only for continuous waves (or pulse waves with a large number of oscillations). The wavelength value for short-time pulse waves (pulse wave with a small number of oscillations) varies due to the broadband nature of the pulse signal.

4.3.2 Inspection Modes

Ultrasonic testing procedures are based on two major inspection modes. These are normal beam inspection and angle beam inspection. The ultrasonic pulse travels through a thickness of material in a normal beam inspection. The so-called *pulse–echo* method requires two transducers. The pulse is generated by the transmitter and captured by the receiver. In contrast, the *pitch–catch* mode involves only one transducer. The pulse generated by the transducer passes trough the material, gets reflected by a boundary and is captured by the same transducer. The angle beam inspection mode introduces refracted shear waves to the monitored specimen. The inspection modes are shown graphically in Figure 4.6.

4.3.3 Transducers

There exist various types of ultrasonic transducers. Most acoustic transducers use piezoelectric ceramics which convert electrical energy into the mechanical energy and vice versa. Figure 4.7 shows a diagram of a typical ultrasonic transducer. The type, size and frequency bandwidth of transducers are important for damage detection resolution. There are various types of transducers used in practice. This includes contact and noncontact transducers. Contact transducers require appropriate coupling (gel, water) for the ultrasound energy transfer. Special types of transducers are used when specimens are immersed in water. Noncontact transducers do not require any coupling but show significant attenuation at high frequencies.

The geometry, frequency and size of the transducers determine the ultrasonic beam near field (Figure 4.8). The following formulas can be used in practice (Rose 1999)

$$\sin\frac{\alpha}{2} = \frac{0.6\lambda}{r} \quad \text{and} \quad N = \frac{r^2 f}{c} \tag{4.4}$$

where α is the angle of divergence, r is the transducer radius and N is the near field distance defined as the point on the axis of the transducer which separates intense oscillations from a smooth decay. A small angle of divergence, required in practice, is a

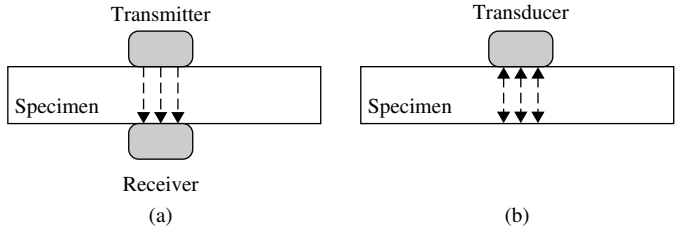

Figure 4.6 Ultrasonic inspection modes: (a) pulse-echo; (b) catch-pitch

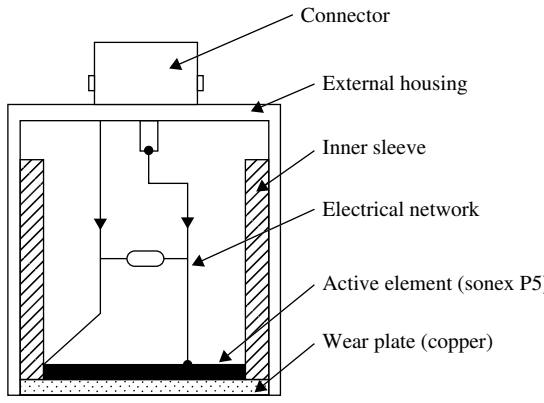

Figure 4.7 Schematic diagram of a typical transducer used for ultrasonic testing

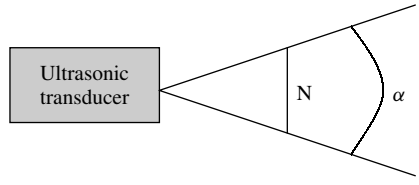

Figure 4.8 Ultrasonic beam near field

compromise between the transducer radius and the input frequency. Often both parameters are decreased in order to reduce destructive interferences in the near field.

Frequency bandwidth is also important since it affects the penetration of the material and damage detection sensitivity. Low-frequency transducers (below 2 MHz) offer better penetration whereas high-frequency transducers (above 15 MHz) provide better sensitivity to small defects.

4.3.4 Display Modes

Ultrasonic data is presented in a form of ultrasonic scans representing damage detection results. Four different types of scans are used in practice. These are:

- *A-scan*: pulse amplitude presented as a function of travel time;
- *B-scan*: two-dimensional representation giving travel time of an ultrasonic pulse versus transducer position;
- *C-scans*: signal echoes are displayed in a top view of the test surface giving defect location maps;
- *D-scans*: a modified C-scan in which time-of-flight values are displayed in a top view on the specimen surface.

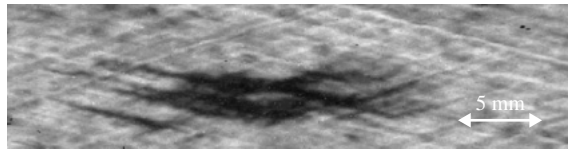

(a)

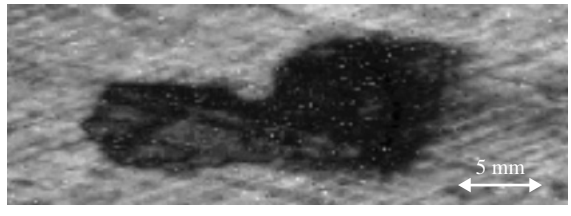

(b)

Figure 4.9 Ultrasonic C-scan examples from a composite plate: (a) delamination after the 2 J impact; (b) delamination after 7 J impact (Pedemonte *et al.* 2001)

Figure 4.9 shows an example of the ultrasonic C-scan for the composite plate with a delamination. The damage is exhibited as the dark area on the plot.

Ultrasonic inspection can be used for a wide range of materials. It is highly sensitive to small defects. However, it requires direct access to inspected surfaces and good inspection skills. Full defects maps (C-scan, D-scan) require scanning and are relatively time consuming. Nevertheless, ultrasonic testing has been used for many years as one of the most successful damage detection techniques.

4.4 ACOUSTO-ULTRASONICS

The acousto-ultrasonic technique is based on stress waves introduced to a structure by a probe at one point and sensed by another probe at a different position. The acousto-ultrasonic method, introduced in the late 1970s (Vary 1988), combines elements of Ultrasonics, guided wave Ultrasonics and Acoustic Emission. All these four techniques utilise stress waves propagating in structures for damage detection. However, Acoustic Emission is the only technique which does not require any external excitation; stress waves are produced by material defects. The other three techniques require an external source of high-frequency excitation to produce stress waves. However, paths of classical ultrasonic waves are well defined and traceable. Similarly, guided wave Ultrasonics is based on well-defined propagation of waves, as described in Section 4.5. In contrast, propagation of acousto-ultrasonic waves is difficult to analyse. This is due to the fact that the method uses high-frequency (usually above 0.5 MHz) impulse excitation which results in a large number of mixed modes. Alternatively, the broadband excitation (Gaussian white noise or sweep sine) could also be used, as reported in (Biemans *et al.* 2001) and shown in Section 4.8.1. Actuating and receiving transducer probes are often not in a line-of-sight position regarding the damage. As a result, the actual transducer responses include not only directly propagating wave modes but also reflected and scattered modes. The rich content of the stress wave energy of complex modes carries a lot of information regarding

possible material and/or structural damage. Figure 4.10 shows an example of an acousto-ultrasonic stress wave from damage detection studies in a composite-metal joint (Kwon *et al*. 2000).

There exist a number of different parameters to describe the stress wave energy. Often AE parameters described in Section 4.2.3 are used in practice. Alternatively, the Stress

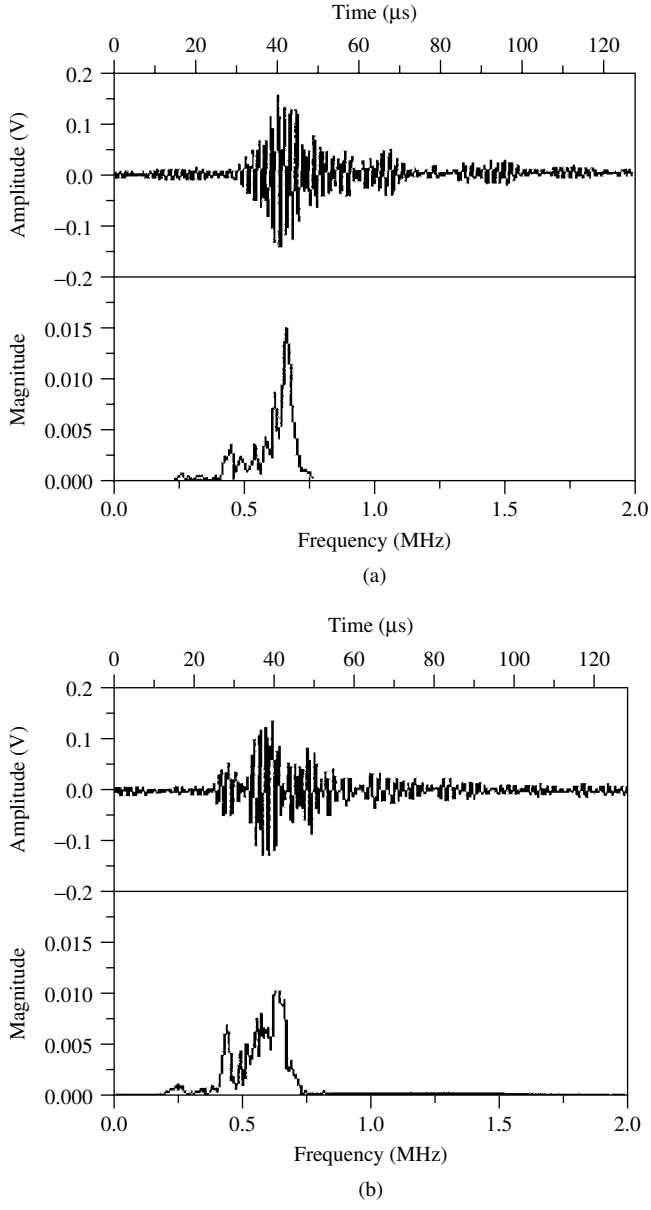

Figure 4.10 Acousto-ultrasonic stress waves from damage detection in a composite-metal joint: (a) unfatigued specimen; (b) fatigued specimen (Kwon *et al*. 2000)

Wave Factor (SWF), based on power spectral density, is applied. The SWF can be defined using spectral moments given as (Kiernanand and Duke 1988)

$$M_n = \int_0^{f_{\max}} S(f) f^n \mathrm{d}f \tag{4.5}$$

where $S(f)$ is the power spectral density, $f_{\max}$ is the maximum frequency of the analysed spectrum and $n = 1, 2, \ldots$.N. The M_0 moment is the most widely used parameter in practice. Figure 4.11 gives an example of this parameter for the acousto-ultrasonic data presented in Figure 4.10.

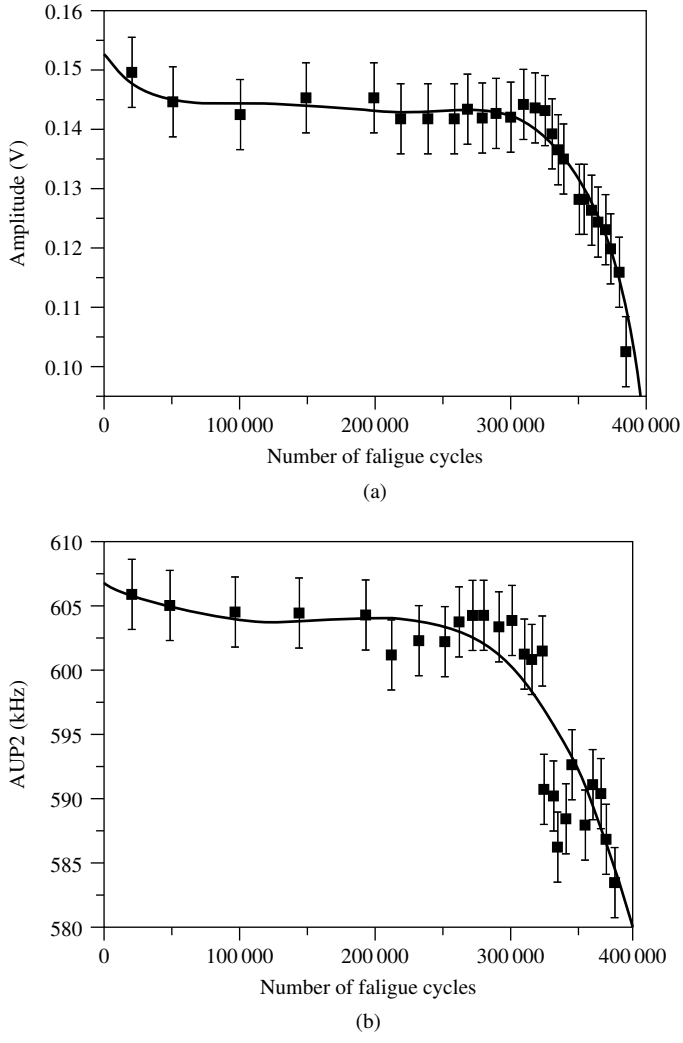

Figure 4.11 Stress wave factors for the data presented in Figure 4.10: (a) peak amplitude; (b) M_1/M_0 (Kwon *et al*. 2000)

4.5 GUIDED WAVE ULTRASONICS

4.5.1 Background

Guided waves are governed by the same wave equations as bulk waves. However, in contrast to bulk waves, they have an infinite number of modes associated with propagation. Guided waves are able to interact with defects in structures due to their propagation properties that are highly sensitive to any discontinuities in materials. This section defines various types of guided waves and briefly introduces Lamb waves which are the most widely used guided waves for structural damage detection.

4.5.2 Guided Waves

Propagating wave packets which are superpositions of various modes are often called guided waves. There are various types of guided waves available in practice. Wave packets, resulting from appropriate stress and strain boundary conditions, which travel on the surface of a solid body, are known as surface waves. Surface waves usually exhibit large amplitudes and travel slower than other types of guided waves.

Rayleigh waves are the best known surface waves (Viktorov 1967). They are nondispersive for uniform material properties. However, their mechanism of propagation is very complex; waves are polarised and surface particles are moved around an ellipse. The components of Rayleigh waves can couple with a medium surrounding the surface of the body. This coupling affects the amplitude and velocity of the wave. The amplitude of the wave decreases rapidly with depth. The rate of decrease depends on the wavelength. Therefore inspection methods based on Rayleigh waves are used mostly to detect surface defects. Other examples of surface waves include Stonely and Love waves. These waves are not commonly used for damage detection and are better known to seismologists than to damage detection experts. Stonely waves occur at an interface between two media. They are closely related to Rayleigh waves. The existence of Stonely waves depends on the density and shear modulus ratios of the neighbouring media. Love waves are horizontally polarized shear waves which also exist on the surface. However, in contrast to the other two types of surface waves they are highly dispersive. Love waves are the fastest propagating surface waves.

Lamb waves (Viktorov 1967) are dispersive plate waves that occur for traction-free forces on both surfaces of the plate. The velocity of these waves depends on the product of frequency of excitation and thickness of the plate. They can propagate long distances and are used for damage detection of plate-like structures. Lamb waves are the most widely used guided waves for damage detection. They are discussed in more details in the next section.

4.5.3 Lamb Waves

Lamb waves refer to elastic perturbations propagating in a solid plate with free boundaries for which the displacements correspond to different basic propagation modes, with symmetric and antisymmetric vibrations. For a given plate thickness d and acoustic frequency

f, there exists a finite number of such propagation modes specified by their phase velocities. A complete description of such propagation characteristics for plates is normally given in the form of a set of dispersion curves, illustrating the plate-mode phase velocity as a function of the frequency–thickness product. Each curve represents a specific mode, which is conventionally called A_0, S_0, A_1, S_1, A_2, S_2, etc. where A_n denotes antisymmetric modes and S_n symmetric modes.

When an excitation is applied at some point on the plate, the excitation energy encounters the upper and lower surfaces of the plate. Longitudinal waves (P) are polarised parallel to the plate whereas shear horizontal waves (SH) form a series of modes. After some time when longitudinal waves are polarised in the direction perpendicular to the surface, shear vertical waves (SV) form modes in connection with P waves; these combined P+SV guided waves are known as Lamb waves.

The most common approach for solving the Lamb wave problem is the method of potentials. For a solid medium bounded by two parallel planes a distance $2d$ apart (see Figure 4.12), the equation of motion, which contains only the particle displacement, can be given as (Achenbach 1984)

$$\mu w_{i,jj} + (\lambda + \mu) w_{j,ji} + \rho f_i = \rho \ddot{w}_i \tag{4.6}$$

where w_i are displacements, f_i are body forces, λ, μ are Lamé constants and ρ is the density. The boundary conditions for the surface tractions can be defined as

$$t_i = S_{ij} n_j \tag{4.7}$$

where t_i are traction forces, S_{ij} are stresses and n_j are cosine directions. The longitudinal and shear waves of plain strain are governed by the well-known wave equations that can be obtained from Equation (4.6) using the Helmholtz decomposition as (Achenbach 1984)

$$\frac{\partial^2 \phi}{\partial x_1^2} + \frac{\partial^2 \phi}{\partial x_3^2} = \frac{1}{c_L^2} \frac{\partial^2 \phi}{\partial t^2} \tag{4.8}$$

$$\frac{\partial^2 \psi}{\partial x_1^2} + \frac{\partial^2 \psi}{\partial x_3^2} = \frac{1}{c_T^2} \frac{\partial^2 \psi}{\partial t^2} \tag{4.9}$$

respectively. Here, ϕ and ψ represent decomposed displacement variables, c_L indicates the velocity of longitudinal wave whereas c_T is the velocity of shear (transverse) waves.

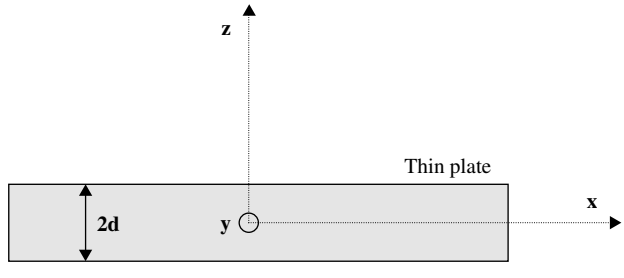

Figure 4.12 Geometry of the plate for Lamb wave propagation

The actual longitudinal and transverse displacements of the plate can be obtained as

$$w_1 = \frac{\partial \phi}{\partial x_1} + \frac{\partial \psi}{\partial x_3} \tag{4.10}$$

$$w_2 = \frac{\partial \phi}{\partial x_3} - \frac{\partial \psi}{\partial x_1} \tag{4.11}$$

respectively. Similarly, stresses can also be expressed in terms of the field variables but are not analysed here. The solutions of Equations (4.8–9), representing travelling waves in the x_1 direction and standing waves in the x_3 direction, can be assumed in the form

$$\phi = \Phi(x_3) \exp[i(kx_1 - \omega t)] \tag{4.12}$$

$$\psi = \Psi(x_3) \exp[i(kx_1 - \omega t)] \tag{4.13}$$

where ω is the frequency and k is the wavenumber. Substituting Equations (4.12–13) into Equations (4.8–9) gives the unknown amplitude functions Φ and Ψ as

$$\Phi(x_3) = C_1 \sin(px_3) + C_2 \cos(px_3) \tag{4.14}$$

$$\Psi(x_3) = D_1 \sin(qx_3) + D_2 \cos(qx_3) \tag{4.15}$$

where

$$p^2 = \frac{\omega^2}{c_L^2} - k^2 \quad \text{and} \quad q^2 = \frac{\omega^2}{c_T^2} - k^2 \tag{4.16}$$

and C_1, C_2, D_1, D_2 are arbitrary constants. Since both field variables involve sine and cosine functions, which are odd and even respectively, the solutions are often split into two symmetric and antisymmetric modes. The displacements for the symmetric modes are

$$w_1 = ikC_2 \cos(px_3) + qD_1 \cos(qx_3) \tag{4.17}$$

$$w_2 = -pC_2 \sin(px_3) - ikD_1 \sin(qx_3) \tag{4.18}$$

whereas the solutions for the antisymmetric modes can be given as

$$w_1 = ikC_1 \sin(px_3) - qD_2 \sin(qx_3) \tag{4.19}$$

$$w_2 = pC_1 \cos(px_3) - ikD_2 \cos(qx_3) \tag{4.20}$$

These equations, known as Rayleigh–Lamb equations for guided waves in plates, show that Lamb wave propagation is generally complex due to the coexistence of at least two modes at any given frequency and the strongly dispersive nature of these modes at high frequency. The traction-free boundary conditions for the plain strain need to be additionally applied in order to obtain the constants C_1, C_2, D_1 and D_2. This leads to Rayleigh–Lamb frequency relations known as the dispersion equations (Achenbach 1984)

$$\frac{\tan(qh)}{\tan(ph)} = -\frac{4k^2pq}{(q^2 - k^2)^2} \tag{4.21}$$

for symmetric modes and

$$\frac{\tan(qh)}{\tan(ph)} = -\frac{(q^2 - k^2)^2}{4k^2pq} \tag{4.22}$$

for antisymmetric modes, where $h = d/2$. The above equations can be solved numerically in order to predict velocities of a propagating Lamb wave of frequency f in a plate of thickness d. The results are presented as a function of the fd frequency–thickness product. Figure 4.13 gives an example of the dispersion characteristics for an aluminium plate. This clearly shows how many complex modes can propagate in the plate. Single S_0 and A_0 Lamb wave modes are possible only for small values of the frequency–thickness product ($fd < 2$).

Furthermore, a single and pure Lamb wave mode may generate a variety of other modes either by interacting with a surface or subsurface flaw or by crossing the interface between two materials of different boundaries. As a result, the problem becomes very difficult to solve analytically. Often numerical analysis is employed to study wave propagation. Figure 4.14 shows a simulated example of the Lamb wave propagating in the aluminium plate with a damage slot positioned in the middle of the plate. Here, the scatter around the damage can be clearly observed in the contour plots of the propagating wave. The study was performed using the Local Interaction Simulation Approach (LISA) (Delsanto *et al.* 1992, 1994, 1997). The method has been proven to perform very well for wave propagation models with complex boundaries, imperfect material interfaces and heterogeneous materials (Agostini *et al.* 2000; Lee and Staszewski 2002, 2003a, 2003b, 2003c).

4.5.4 Monitoring Strategy

Real engineering structures under inspection are usually quite complex when compared with simple plates studied in laboratory conditions and reported in the literature. The

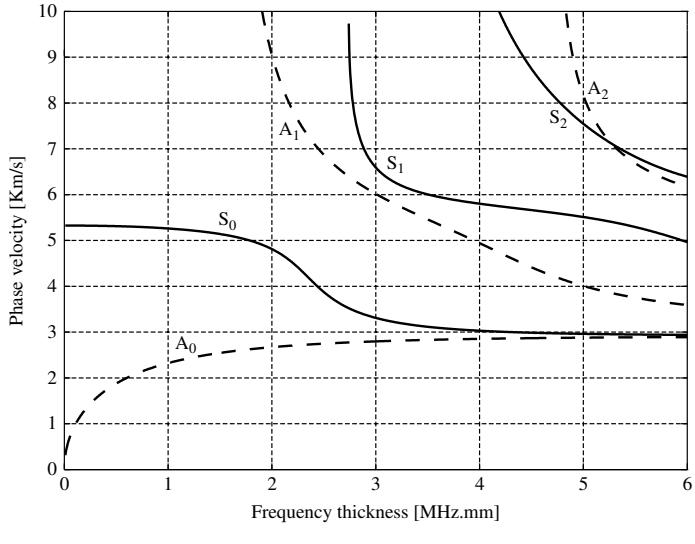

Figure 4.13 Lamb wave dispersion characteristics for an aluminium plate

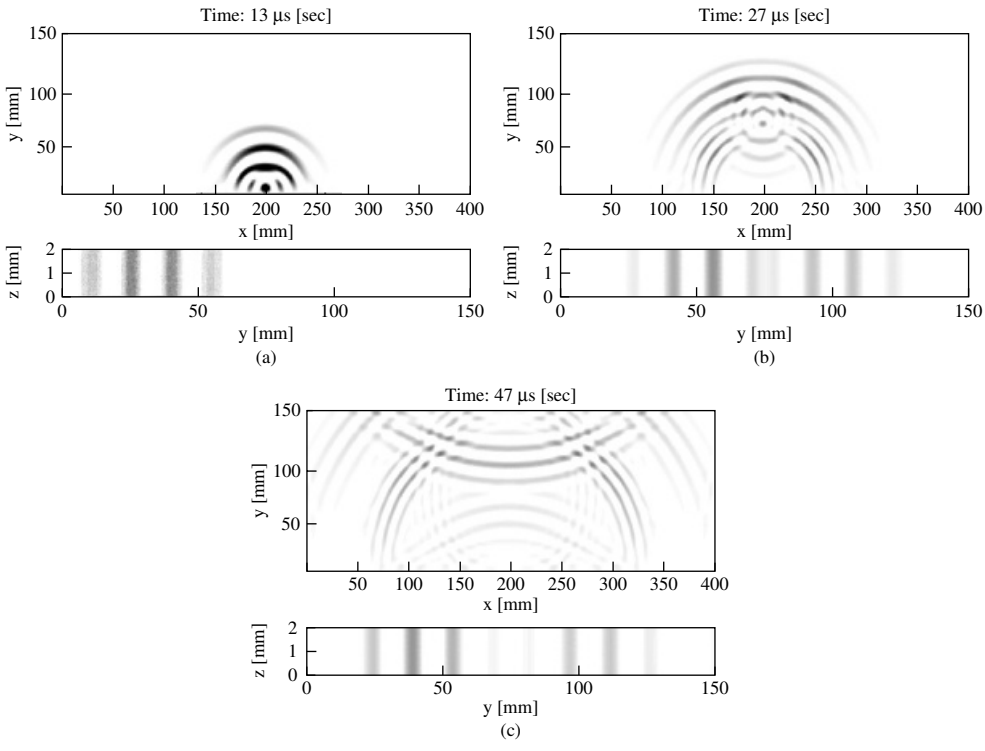

Figure 4.14 Snapshots of the S_0 Lamb wave mode propagation in an aluminium plate with a damage slot after: (a) 13 μs; (b) 27 μs; (c) 47 μs. The figure shows out-of-plane (top parts) and in-plane (bottom parts) vibration (Lee and Staszewski 2003a)

complexity is determined by various types of joints, stiffeners, rivets, complicated shapes or varying thickness. This causes the entire analysis to be much more complicated and requires an appropriate monitoring strategy.

The methodology or strategy of monitoring is extremely important for successful damage detection. The basic factors, which determine the Lamb wave based damage detection analysis are related to properties of the structure under inspection, transducer schemes, choice of excitation input signal, and appropriate signal processing, as reported in (Wilcox *et al.* 1999; Staszewski and Boller 2002). Other elements include various aspects related to transducer coupling methods, optimal sensor locations and sensor validation procedures. The last but not least is the hardware used for monitoring, graphical interface and data storage organisation.

The dispersive nature of Lamb waves and also the finite number of modes at a given frequency makes long-range inspection very difficult. To overcome these problems, low frequency–thickness products are often utilised for damage detection. In this case only two fundamental modes A_0 and S_0, are used. It is important to limit the bandwidth of the excitation to a range over which there is little dispersion (i.e. the phase velocity does not change significantly with frequency).

The first applications of Lamb waves for damage detection used bulky wedge (angle-beam) transducers. It appears that piezoceramic elements are now the most widely used transducers due to the fact that they can be used as sensors and actuators at the same time. Often piezoceramics can become an integral part of the monitored structure, as shown in Section 4.6.1. Recent advancements in this area include optical fibre sensors (Betz *et al*. 2002) and MEMS (Micro-Electro-Mechanical Systems) sensors (Khuri–Yakub *et al*. 2000). Both types of sensors can be used not only for Lamb wave detection but also for strain measurements. MEMS devices can additionally generate Lamb waves. A number of different practical aspects need to be considered once choosing transducers for Lamb wave detection. This includes coupling, connectors and environmental protection. The cold bonding is usually preferred to hot bonding. The process of bonding must be as easy (if not easier) as the procedure for bonding strain gauges. Also, bonded sensors are better than embedded due to possible sensor failures and replacements. Reliable connectors and environmental protections are required to prevent sensor failures. Wireless applications are possible with piezoceramic and MEMS sensors. Coupling, connectors and environmental protection are particularly important in the case of optical fibre and piezoceramic sensors.

Different types of signals are used as input excitation. It is considered that the simpler the input signal the simpler the output signal for damage detection. The choice of input excitation is often a compromise between the amplitude and the mode generation. Low-voltage signals are possible when the input frequencies are within transducer resonance frequencies (see Section 4.6.3). This is often associated with intelligent signal processing to remove undesired modes and extract features related to damage. In practice transducers resonance frequencies do not coincide with single Lamb wave mode frequencies.

Previous studies (Biemans *et al*. 2001; Staszewski *et al*. 1999a) show that even simple input signals can lead to complex output signals due to various attenuation and dispersion effects which are not related to damage. This clearly shows that intelligent signal processing is one of the most important elements of the Lamb wave based damage monitoring strategy. Examples of various signal processing techniques for damage detection are discussed in Chapter 5.

Once the transducers excitation signals are chosen the question is where to put sensors for optimal damage detection. Recent years have shown considerable progress on the problem of determining the number and location of sensors in engineering structures. Some of these techniques are discussed in Chapter 5.

4.6 PIEZOELECTRIC TRANSDUCERS

4.6.1 Piezoelectricity and Piezoelectric Materials

Piezoelectric transducers are the most widely used sensors for damage detection based on sound and ultrasound. Piezoelectricity is an electric polarisation effect due to mechanical forces. In other words an electric charge is collected on the surface of the piezoelectric material when it is squeezed.[1] Often the converse effect is possible, i.e. the material generates a mechanical strain in response to the applied electric field. Both effects are illustrated graphically in Figure 4.15. Piezoelectricity was discovered by Jacque and Pierre

[1] *Piezo* is in fact a Greek term for *to squeeze*.

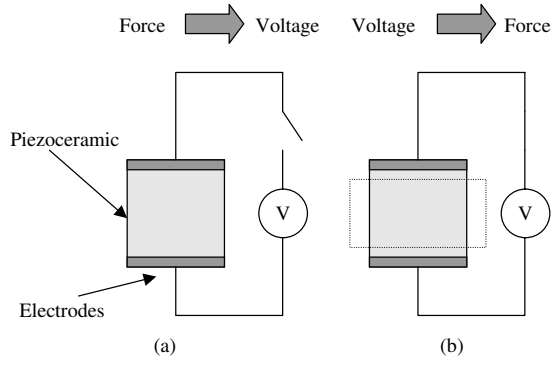

Figure 4.15 Direct (a) and inverse; (b) piezoelectric effects

Curie in 1880s. It is an anisotropic property of crystalline materials and results from nonuniform charge distributions within a crystal's cells. There are number of different materials which exhibit these effects. Natural materials include quartz (SiO_2), Rochelle salt and tourmaline. The quartz crystal exhibits stiffness comparable to steel and shows high voltage sensitivity. Manufactured piezoelectric ceramics were introduced in the early 1950s. The first material developed with piezoelectric properties was barium titanate ($BaTiO_3$). The two most widely used manufactured materials are lead zirconate titanate (PZT) and polyvinylidene fluoride (PVDF). The former is a ceramic and the later is a polymer film. Piezoelectric ceramics (often called piezoceramics) are quite brittle and need to be handled with care. Piezoelectric polymer films are, in contrast, very flexible and easy to handle for sensor applications. PVDF exhibits the strongest known piezoelectric behaviour of all polymers. PVDF offers better direct piezoelectricity and worse inverse piezoelectricity than the PZT, and therefore it is more often used for sensing applications.

Piezoceramic materials have been used for various types of transducers for many years. Recent years have shown extensive progress in developing sensing devices. The adaptation and integration of piezoceramic sensors onto, or into, structures has become more feasible. Low-profile piezoceramic sensors with wrap-around electrodes are available as thin plates and discs which can be bonded, and/or embedded, in monitored structures. Other important developments in this area include piezoceramic paints (Egusa and Iwasawa 1993), Smart Layers™ (Chang 1998) and piezoceramic fibres (Yoshikawa *et al.*). Smart Layers™ are Kapton dielectric films with an embedded network of distributed piezoceramic PZT sensors. These layers can be fabricated in various sizes and shapes, as shown in Figure 4.16.

Piezoceramic sensors are particularly attractive for structure integrated damage detection since they exhibit simultaneous actuator and sensor behaviour. This allows for both passive and active damage detection. In fact the majority of damage detection applications based on guided wave ultrasonic utilise PZT type sensors. There exist a vast amount of literature related the properties and behaviour of piezoceramic elements.

4.6.2 Constitutive Equations

Piezoelectric materials exhibit both mechanical and electrical properties. It is well known that mechanical properties of any linear elastic material can be described by the Hooke's

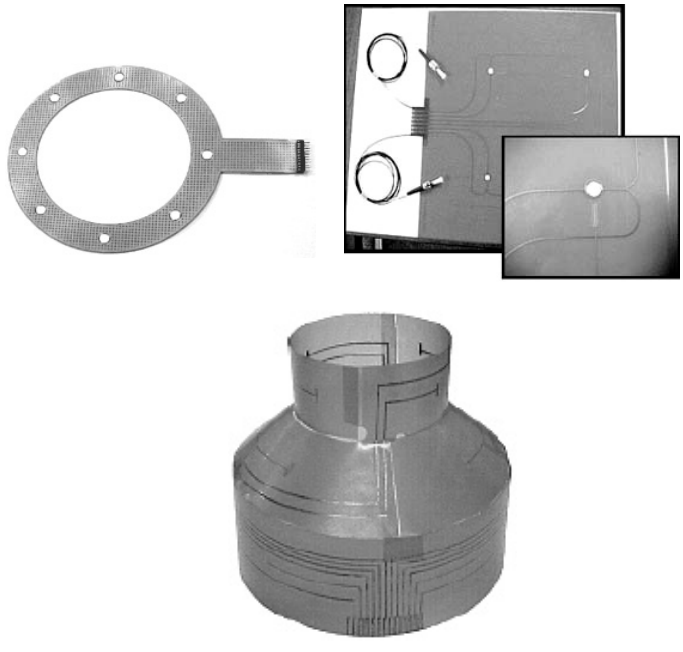

Figure 4.16 Smart Layer™ sensors. (Courtesy of Acellent Technologies Ltd, California)

law which gives the relationship between strain S and stress T

$$S = cT \tag{4.23}$$

where c is the compliance characterising the material. By analogy, a similar relationship exists to describe electrical properties of dielectrics. It shows how the electric displacement D changes as a result of the electric field E applied

$$D = \varepsilon E \tag{4.24}$$

where ε is the permittivity. The electric field E is equivalent to a force field in mechanics and represents the work done against the electric field in order to move a charge. In contrast, the electric displacement D gives the redistribution of charge when the material is subjected to an electric field. Equations (4.23) and (4.24) are often called constitutive mechanical and electrical equations, respectively. Piezoelectric materials exhibit coupled mechanical, electrical and piezoelectric properties. The constitutive equations describing these materials can be given as

$$\begin{aligned} S &= S_E T + d^t E \\ D &= \varepsilon_T E + dT \end{aligned} \tag{4.25}$$

where S is the mechanical strain, E is the electric field, T is the mechanical stress, D is the electrical displacement (all these state variables are second-order tensors), d is the

piezoelectric coefficient and ε is the permittivity. Here, subscripts E and T indicate that the quantities are under constant (usually zero) electrical and stress fields, respectively. Additionally, superscript t indicates the transpose. Equation (4.25) gives the strain–charge form of the constitutive equations which relate the electric and mechanical fields. The other three forms give rearranged relationships between the state variables. The constitutive equations describe how voltage changes in the material when the charge moves, and the other way around.

Piezoelectric coefficients d_{ij} defined as

$$d_{ij} = \frac{strain}{applie\ delectric\ field} = \frac{charge\ density}{applied\ stress} \tag{4.26}$$

characterises either the strain produced by an applied electric field or the charge density developed from the applied stress field. The subscript i indicates the direction of electric field or displacement, whereas the subscript j gives the direction of strain or stress. The axis notation can be chosen as shown in Figure 4.17; $i, j = 1, 2$, and 3 indicate the shear strains associated with directions 1, 2 and 3, respectively. Figure 4.18 illustrates the physical interpretation of the piezoelectric coefficients. Here, the electric field E_3 is applied to the transducer of thickness t and width w. The transducer expands vertically (in the direction indicated by the subscript 3) by the factor equal to $1 + \varepsilon_3$; the new thickness of the transducer becomes $t(1 + \varepsilon_3)$. At the same time the transducer shrinks horizontally (in the direction indicated by the subscript 1) by the factor equal to $1 - \varepsilon_1$; the new width of the transducer becomes $w(1 - \varepsilon_1)$. The piezoelectric coefficients are then equal to

$$d_{33} = \frac{\varepsilon_3}{E_3} \quad \text{and} \quad d_{31} = \frac{\varepsilon_1}{E_3} \tag{4.27}$$

Note that d_{31} is in this case a negative number.

Often the conversion between the electrical and mechanical (or mechanical and electrical) energies is described using the electromechanical coupling coefficient k_{ij} which is defined as

$$k_{ij}^2 = \frac{stored\ electrical\ energy}{applied\ mechanical\ energy} = \frac{stored\ mechanical\ energy}{applied\ electrical\ energy} \tag{4.28}$$

where the subscript notations are identical to the convention used for piezoelectric coefficients. This parameter describes the efficiency of the energy conversion.

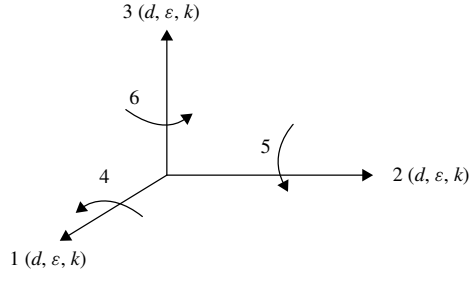

Figure 4.17 Axis notation for the strain/stress and electric fields

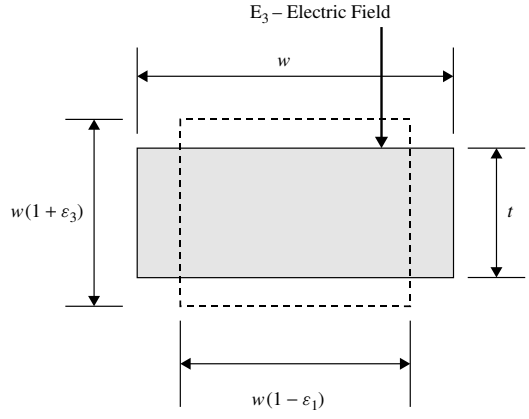

Figure 4.18 Physical interpretation of piezoelectric coefficients

4.6.3 Properties

The manufactured piezoceramics are initially isotropic. They are composed of randomly oriented cells which are polarised when the strong DC current is applied. This process is called poling due to the fact that electric dipoles are permanently aligned by the electrical field. In contrast to natural piezoelectric materials, piezoceramics show high charge sensitivity.

The voltage–strain behaviour of piezoceramics is in general nonlinear. Only the linear part of the voltage–strain curve is used in practice for sensing. Most piezoceramics also exhibit a typical hysteretic behaviour which exhibits the energy loss.

All piezoceramic materials have operating limits associated with temperature and voltage. The piezoelectric properties are exhibited below the so-called Curie temperature. When this temperature is reached or exceeded the material is not piezoelectric anymore, i.e. electric dipoles change their orientations. Some piezoceramics can operate up to 550 °C. The properties of piezoceramic materials also change as a result of temperature. Figure 4.19 shows an example of the experimental peak-to-peak voltage amplitude as a function of the temperature. The excessive voltage (usually above 1000 V) has a similar depolarising effect. Piezoceramic materials are also very brittle. High level of tensile stress can lead to mechanical damage and depolarisation.

The impedance can be used in order to describe dynamic properties of the piezoceramic transducers. The maximum performance of the transducer is achieved when the excitation frequency is chosen as one of the natural resonance frequencies of the transducer. This enables a very efficient conversion from the electrical to mechanical energy. Resonance frequencies are associated with different vibration modes of the transducers. These modes can be used for the generation of different types of waves. Often Frequency Response Functions (FRF) and transfer characteristics are obtained for the transducers using theoretical and experimental studies. Various piezoceramic elements available in the standard Finite Element (FE) codes can be used for the theoretical analysis. Figure 4.20 gives an example of such analysis for a simple disc-type transducer. Here, the strongest radial and thickness modes are identified. It is clear that resonance frequencies of the

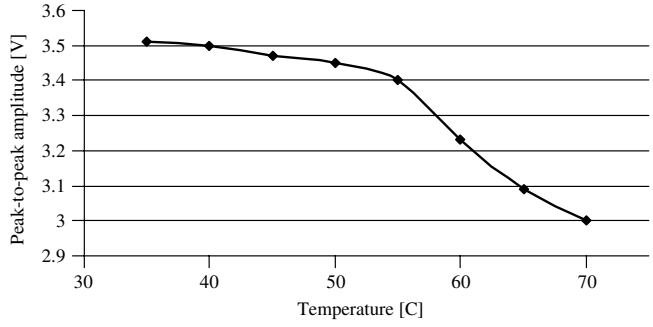

Figure 4.19 Temperature effect on Lamb wave responses when monitored with piezoceramic sensors

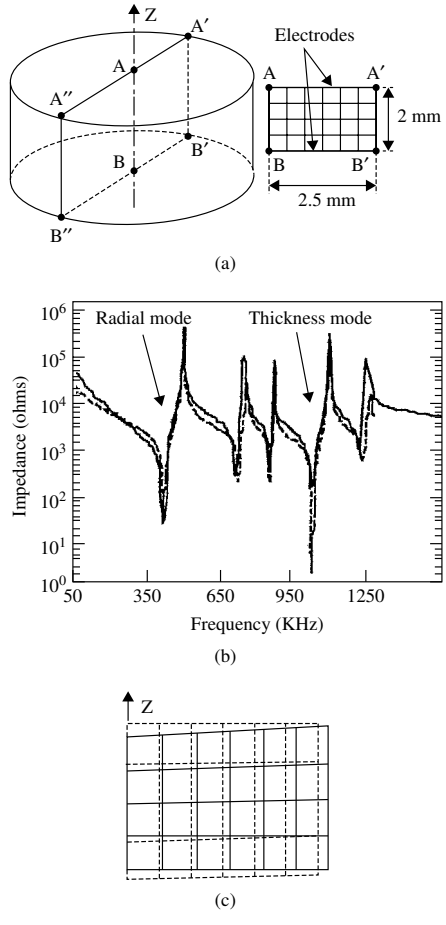

Figure 4.20 Piezoceramic transducer characterisation using modal analysis: (a) model geometry; (b) transfer functions: solid line – experimental curve, dashed line – numerical simulation; (c) vibration modes (Moulin *et al*. 1997, reproduced by the permission of The American Institute of Physics)

embedded or bonded transducers will be influenced by the acoustical loading conditions associated with the boundaries.

4.7 PASSIVE DAMAGE DETECTION EXAMPLES

4.7.1 Crack Monitoring Using Acoustic Emission

Acoustic Emission analysis was performed on a full scale *Airbus A320* aircraft inner wing as a part of the certification procedure. Figure 4.21 shows a schematic diagram representing the specimen on a fatigue test rig. The location of Acoustic Emission sensors is given in Figure 4.22 together with the three dimensional geometry of the analysed part of the wing. The data from sensors located in different planes allow for estimating the true position of the acoustic source due to fatigue crack damage. The signal amplitudes from the source varied between 55 and 100 dB with the majority of results around 90 dB after distance amplitude correction. Figure 4.23 gives an example of the variation of Acoustic Emission amplitude with distance in metres. All noncrack noises that come

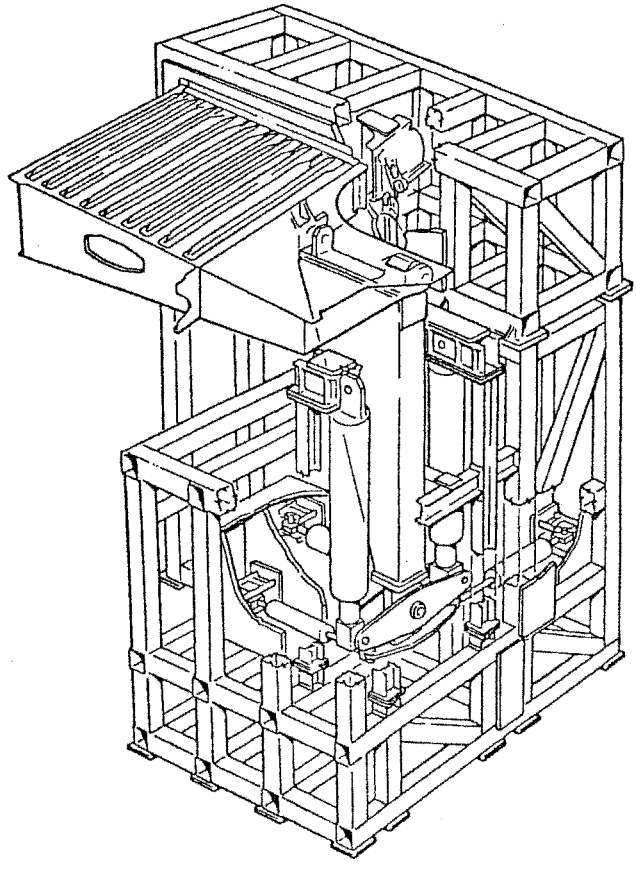

Figure 4.21 Schematic diagram representing the wing specimen on a fatigue test rig

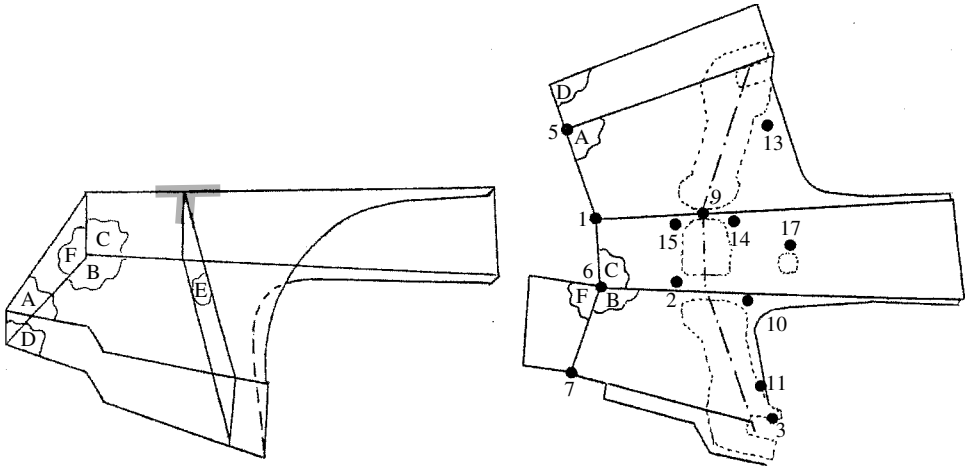

Figure 4.22 Three-dimensional geometry of the analysed part of the wing together with the Location of Acoustic Emission sensors

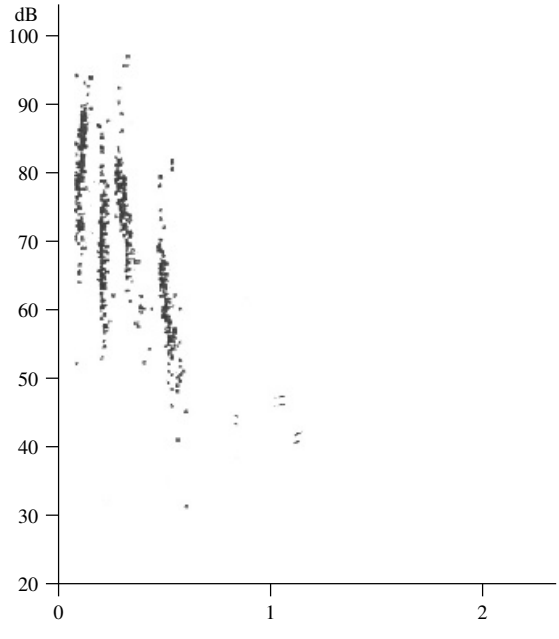

Figure 4.23 Example variation of Acoustic Emission amplitude with distance in metres

from background, fretting, etc., were eliminated before any source location studies. The analysis of the data established within 50 cycles showed the conclusive evidence of the presence of cracks and was used to direct conventional NDT to the locations. The growth of the length of the cracks was also monitored and showed that the five cracks that were detected could be monitored contemporaneously.

The results showed that Acoustic Emission could detect stress waves that emanate from growing cracks that occurred during full-scale fatigue tests.

4.7.2 Impact Damage Detection in Composite Materials

This section presents impact damage detection results from the passive monitoring approach utilising piezoceramic sensors (Staszewski *et al*. 1999b). The experimental tests involved a series of impacts on a simple composite structure shown in Figure 4.24.

The two specimens used in the experimental investigations were rectangular composite panels (530 × 225 mm) fabricated from the T300/914 carbon/epoxy unidirectional prepreg using nominal thickness of 0.15 mm/ply. They were made from 32 plies, except for the area at the root which was 48 plies, and the lay-up sequences were $[+45, -45, 0_4, +45, -45, 0_4, +45, -45, 0_2, 90_2, 0_2, -45, +45, 0_2]_s$ and $[-45, +45, 0_3, -45, +45, 0_2, +45, -45, 90_2, -45, +45, O]_s$, respectively. A ply build-up region was fabricated to simulate a reinforcement. A composite stiffener was bonded to the root side of the panel. The padded area allowed for the effects of ply drop-offs on the detection procedure to be investigated. The stiffener allowed for a disbond to be analysed. The composite panels were representative of aircraft wing skin parts. The panels were instrumented with one piezoceramic *PZT Sonox P5* plate (15 × 15 × 1 mm) bonded to the root side, as shown on a schematic diagram in Figure 4.25. The composite panel was mechanically fastened to a stiffening aluminium subframe using screws. This allowed for the quick replacement of the analysed plates. The composite panel was attached to the metal loading frame, as shown in Figure 4.26.

The composite/aluminium structure was statically loaded (0.2 kN, displacement equal to 18 mm) as a cantilever beam using a *Schenck* 250 kN servo-hydraulic test machine. The functionality of the sensor was checked using low energy 2 J impacts at random positions

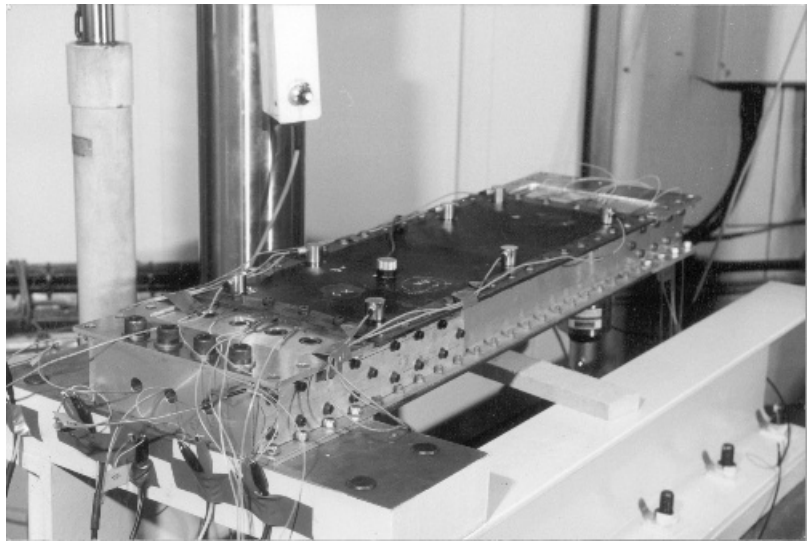

Figure 4.24 Composite structure representative of an aircraft wing skin

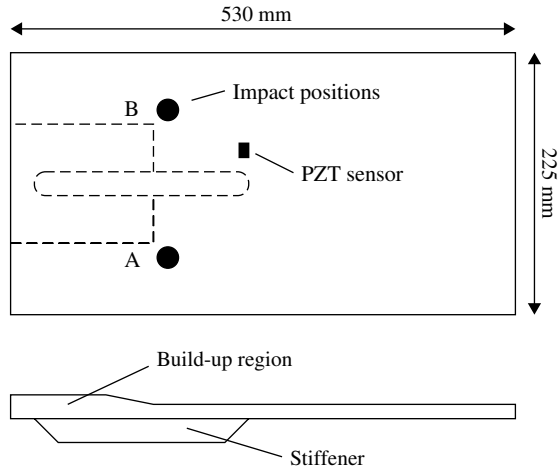

Figure 4.25 Schematic diagram of the composite panel (Staszewski *et al*. 1999)

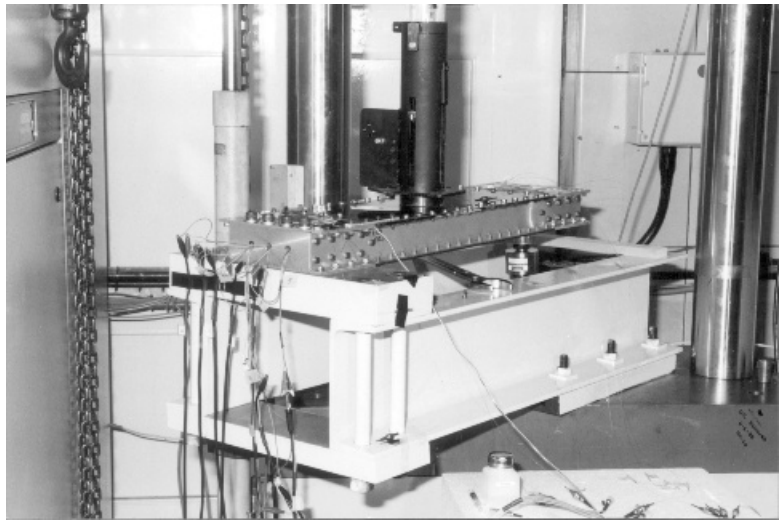

Figure 4.26 Loading arrangements for the wing-box structure (Staszewski *et al*. 1999)

on the plate. A mobile impactor was used in the tests. This initial study was followed by a series of test impacts at positions A and B (Figure 4.25) with the energy levels equal to: 2, 4, 8, 12, 20 J for impact location A; and 2, 4, 8, 12, 16, 24 J for impact position B. The panel was A-scanned after each impact to check for possible damage. The presence of clear delamination was observed after the 20 and 24 J impact at position B.

The impact strain data were acquired from the piezoceramic sensor using a digital 2-channel *HP* oscilloscope with a sampling frequency of 400 kHz. An example of the strain data for the 4 J impact at position B is given in Figure 4.27. The absolute maximum values of the strain data are given in Figure 4.28. The results show that in general the

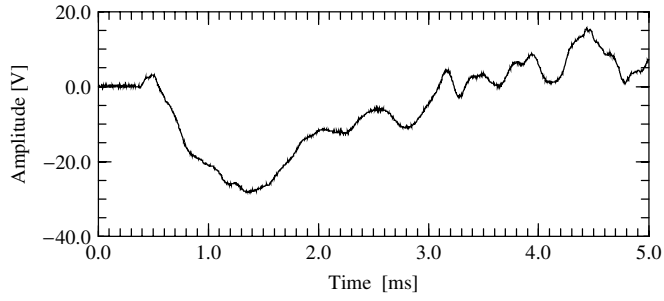

Figure 4.27 Impact strain data for the 4 J impact at position B (Staszewski *et al.* 1999)

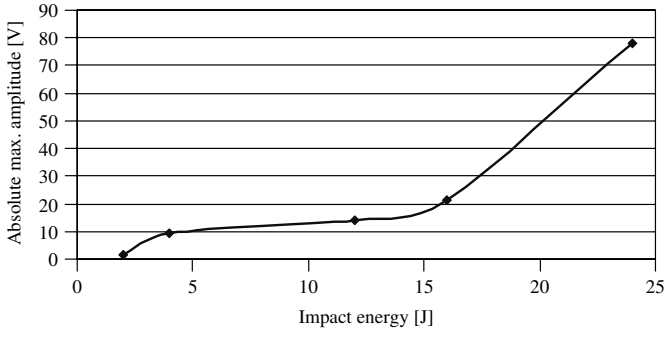

Figure 4.28 Absolute maximum values for the impact strain data

characteristics increase with the impact energy. Thus impact energy levels can be estimated analysing the strain data obtained from the piezoceramic sensor. These energy levels can be related to possible damage severities in the composite panels. Further analysis examples using advanced signal processing techniques are given in Chapter 5.

4.8 ACTIVE DAMAGE DETECTION EXAMPLES

4.8.1 Crack Monitoring in Metallic Structures Using Broadband Acousto-Ultrasonics

A simple fatigue experiment was performed in order to obtain the strain data from metallic specimens with growing cracks (Biemans *et al.* 2001). The specimens used were two rectangular (400 × 150 × 2 mm) aluminium plates with cracks initiated by spark erosion in the middle of the plates. Figure 4.29 shows the experimental set-up. The fatigue test was performed on a *Schenck* 250 kN servo-hydraulic test machine running in load control. The aluminium specimens were subjected to three different load conditions:

- *no load* – close to 0 kN;
- *static load* – at 12.5 kN mean load;
- *dynamic load* – static load plus sinusoidal tension–tension cycling loading with a frequency of 6 Hz and maximum amplitude of 11.5 kN.

Figure 4.29 Experimental set-up for crack monitoring using acousto-ultrasonics (Biemans *et al*. 2001)

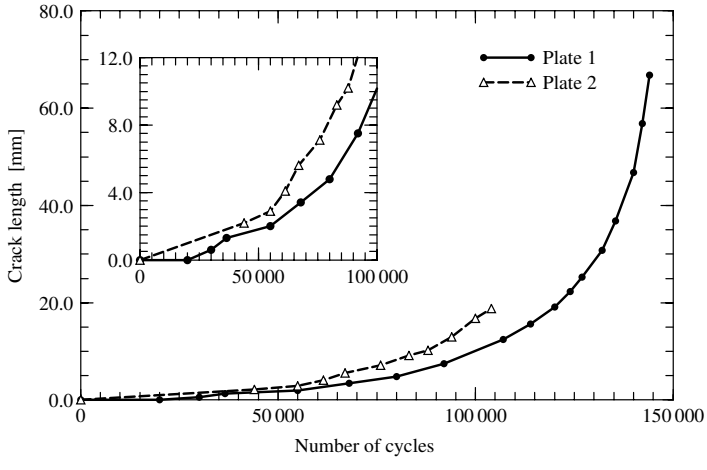

Figure 4.30 Crack propagation curve (Biemans *et al*. 2001)

Crack lengths were determined using a microscope to an accuracy of 0.01 mm. Figure 4.30 shows an example of a crack propagation curve for the analysed specimens.

Each plate was instrumented with six piezoceramics (PZT material *Sonox P5*; dimensions: $15 \times 15 \times 1$ mm) bonded in a symmetrical configuration 20 mm below and above the initiated crack, as shown in Figure 4.31. The piezoceramic no. 2 on each plate was used as an actuator in order to perform the acousto-ultrasonics damage detection.

The study involved two different types of excitation:

1. Gaussian white noise with the maximum frequency of 16 kHz;
2. sine sweep from 10 to 50 kHz with the ramp time of 0.01 s.

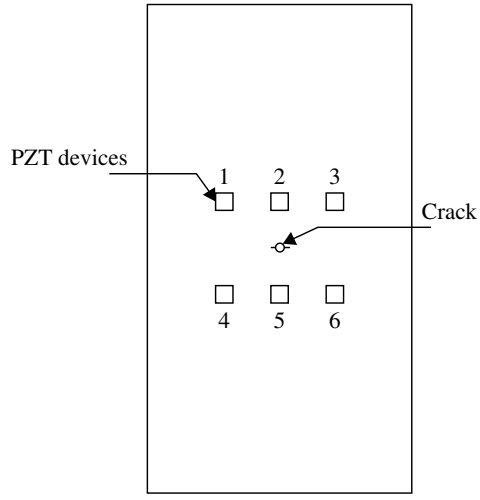

Figure 4.31 Sensor locations on the aluminium specimen used in crack monitoring tests (Biemans *et al*. 2001)

The maximum amplitude of excitation was equal to 20 V. The signals were generated using the *DIFA SCADAS II* and *Philips PM5138* generators.

The piezoceramics 5 and 6 were used to monitor the growing cracks. The response data, from the piezoceramic sensors no. 5 and 6, were recorded by a *DIFA SCADAS II* 24 channel measuring system running the *LMS 3.4.04* data acquisition software and by a digital 2-channel *Tektronix TDS 210* oscilloscope. Figure 4.32 shows an example of the piezoceramic response to the sine sweep excitation for different types of load used in the experiment. Here, a clear drift can be observed for the dynamic load due to the 6 Hz tension–tension cycling loading.

Various signal parameters were estimated for the analysed data. Figure 4.33 gives the results obtained for the minimum amplitude values, for plate no. 5 under the sweep sine excitation. Results, obtained for the *static load* condition, show a fairly linear behaviour while for the *no load* condition a similar linear relationship can only be observed after a certain crack length. The results obtained with monitoring under the *dynamic load* are quite arbitrary. Performing, however, a linear regression over these data may possibly lead to a result similar to the data for the *no load* and *static load* conditions. The reason for the relatively good result when monitoring under the *static load* condition can be seen in a clear situation of the crack being fully open. For the other two load conditions the situation of the crack looks likely to be less clear.

The experimental data were also analysed using the classical Fourier transform approach. Examples of power spectra for the data from sensor no. 5 are given in Figure 4.34. Here, two dominant spectral components at about 1.5 and 2.7 kHz can be observed in Figure 4.34a for the data representing the undamaged plate. The amplitude of these two components decreases when the crack grows in the plate, as shown in Figure 4.34b and 4.34c, whereas the remaining parts of the spectrum are relatively unchanged. The results show that any direct comparison of spectra requires further signal processing analysis. A number of spectral statistical parameters, discussed in Chapter 5, were calculated for the sensor data under the

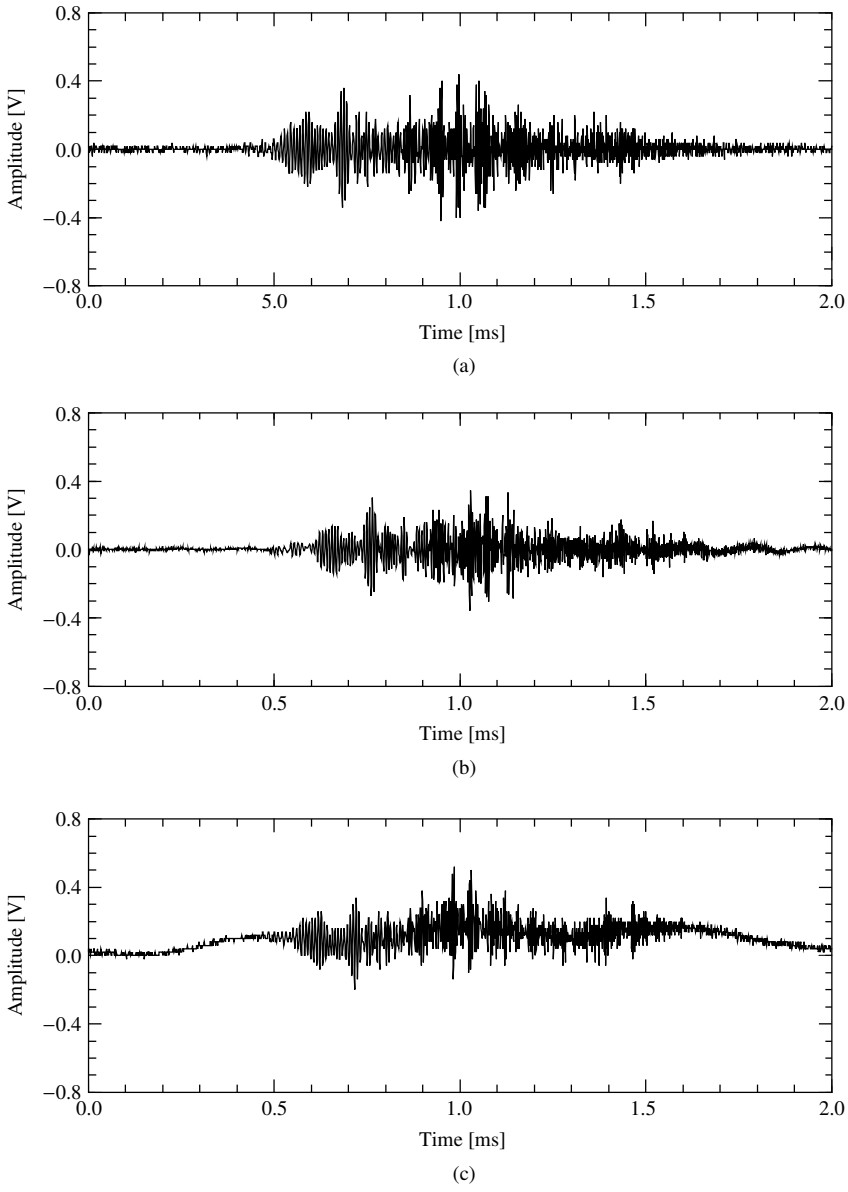

Figure 4.32 Acousto-ultrasonic responses to sine-sweep excitation for: (a) no load; (b) static load; (c) dynamic load (Biemans *et al*. 2001)

sine sweep excitation. Figure 4.35 shows an example of the Root Mean Square (RMS) of Spectral Difference characteristics for sensor no. 5. Again, results obtained for the *static load* condition show a monotonic behaviour while for the *no load* and *dynamic load* conditions the results are not satisfactory – the curves do not indicate any crack growing in a plate. More examples related to these investigations are given in (Biemans *et al*. 2001).

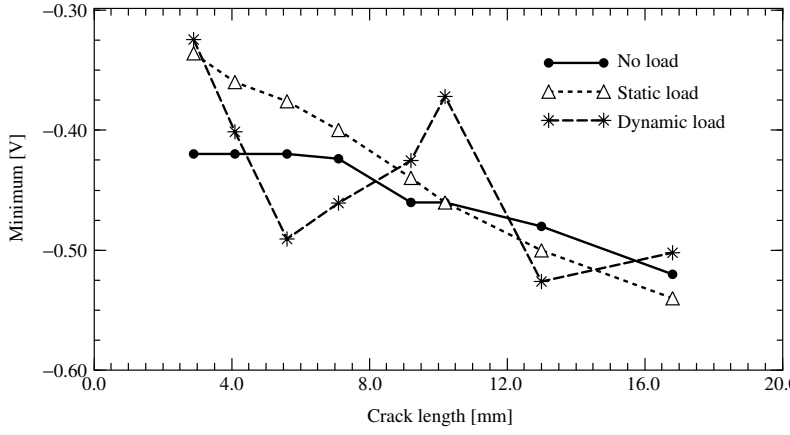

Figure 4.33 Minimum amplitude values for the acousto-ultrasonic responses (Biemans *et al*. 2001)

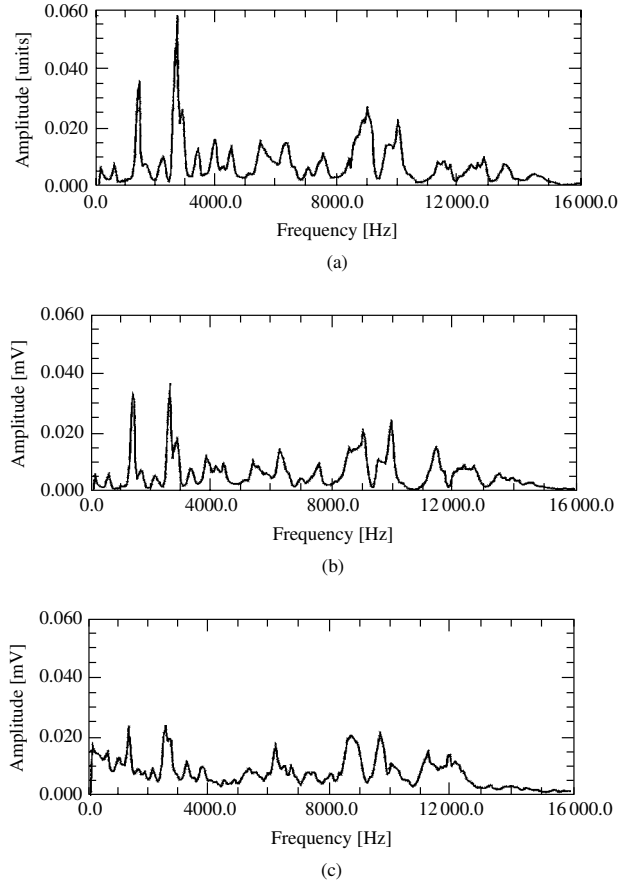

Figure 4.34 Power spectra for acousto-ultrasonic data acquired under the sine sweep excitation: (a) undamaged plate; (b) crack length – 12.5 mm; (c) crack length – 66.8 mm (Biemans *et al*. 2001)

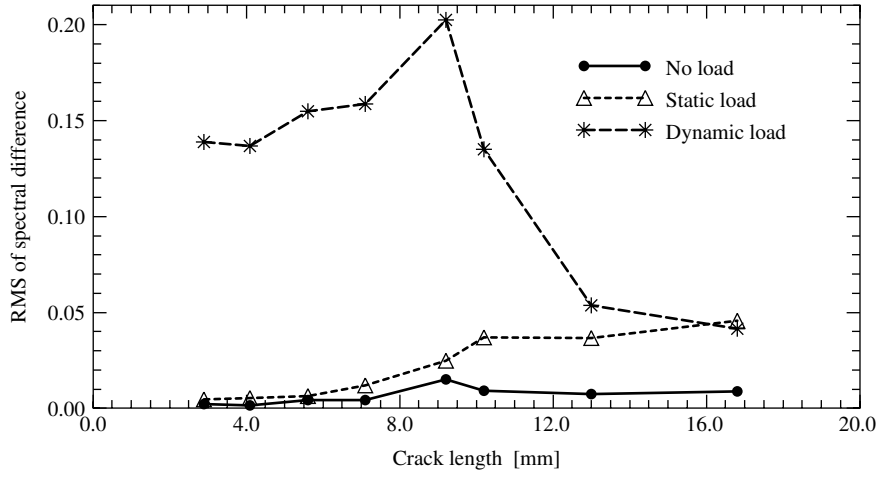

Figure 4.35 Root Mean Square for the Spectral Difference values for the sweep sine excitation (Biemans *et al*. 2001)

This preliminary study shows that satisfactory damage detection results can be obtained under all analysed load conditions. However, this requires the appropriate choice of excitation and signal processing. Also, the best results are mainly obtained under the *static load* when cracks tend to be clearly open or under the *dynamic load* when cracks open and close successively due to cycling loading.

4.8.2 Impact Damage Detection in Composite Structures Using Lamb Waves

This section presents damage detection analysis based on Lamb waves. The study involves the composite wing-box structure described in Section 4.7.2. Piezoceramic sensors have been used to introduce the excitation signals and to acquire the Lamb wave responses. The sensors chosen for these tests were $3 \times 4 \times 1$ mm piezoceramic P160 plates. A general rule of ultrasound excitation is to excite the actuator at its natural resonances rather than at any other frequency. This approach enables a very efficient conversion from the electrical to mechanical energy, as discussed in Section 4.6.3.

A two-dimensional numerical model was developed (Assaad *et al.* 1990) using the ATILA FE code in order to perform the modal and harmonic analysis of the piezoelectric transducers. The analysis resulted in four natural vibration modes for the frequency bandwidth between 100 kHz and 1 MHz. The second mode at 400 kHz was the best electromechanically coupled ($k_e = 43\,\%$). The computation of the displacement field, shown in Figure 4.20, shows that the analysed mode of vibration is a transverse mode.

The transducers have been positioned in various locations in order to detect different types of damage (e.g. impact damage, delaminations, substructural disbonds). Figure 4.36 shows sensor locations on the composite structure. A series of impacts, as described in Section 4.7.2, was performed in order to introduce various severities of damage to the composite skin. A pair of transducers, i.e. El (actuator) and R1 (sensor), was used to allow

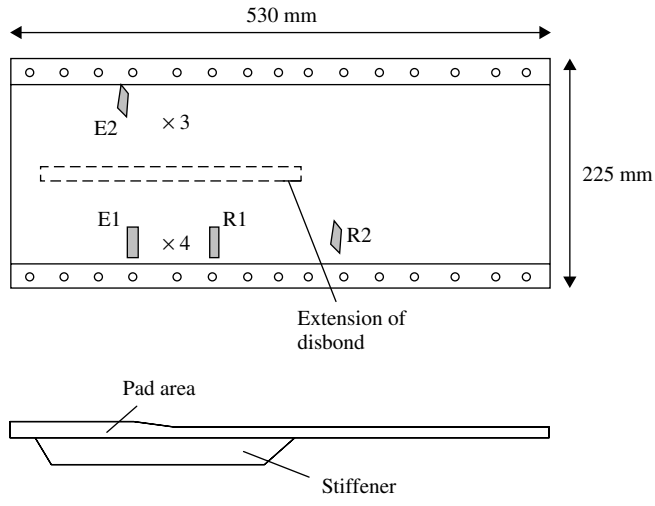

Figure 4.36 Impact positions and locations of Lamb wave transducers on the composite wing-box structure

for the inspection of the plate near impact location 4 (see Figure 4.36). One more pair of transducers, i.e. E2 (actuator) and R2 (receiver), were positioned in order to monitor the disbond growth between the stiffener and the composite plate under cyclical loading and detect possible delaminations at impact location 3 (see Figure 4.36).

A pulse 5-cycle sine burst signal at 400 kHz used to excite the actuators at their resonance frequencies. The Lamb waves excited by the actuators propagated along the plate and were received by the sensors. The responses were amplified, filtered and transferred to a digital oscilloscope. The data acquisition utilised 64 averages in order to improve the signal-to-noise ratio.

Preliminary tests have been performed on the structure in order to study the influence of external conditions, such as additional vibration and temperature, on Lamb wave testing procedure. This was followed by a sequence of testing steps:

- acquisition of Lamb wave signals before the tests (*no damage* condition);
- specimen loaded under 0.2 kN: acquisition of Lamb wave signals;
- vibration conditions: acquisition of Lamb wave signal during, the tests;
- impact tests performed with a mobile impactor using different energy levels (2 J, 4 J, 8 J, 12 J, and 24 J) in location 3 and 4: after each impact, inspections of the plate with Lamb waves were carried out;
- cyclic loading with different displacement levels (9 ± 7 mm, 14 ± 9 mm, 20 ± 12 mm, 22 ± 15 mm): acquisition of Lamb wave signals during the tests.

The first set of tests has demonstrated good reproducibility of the Lamb wave responses under external conditions (external vibration and loading). The performance of all the sensors was not affected by varying thermal conditions; Lamb wave responses remained unchanged after the thermal tests.

The second set of tests was performed in order to measure the sensitivity of Lamb wave signals to damage (delamination and disbond). Damage detection analysis utilised the presence of other modes, or modes conversion due to possible discontinuities in the structure.

Figure 4.37a shows the Lamb wave response from sensor R1 in the absence of defects. Here, the first wave packet was identified as the S_1 mode from a measurement of its group velocity using the time-of-flight analysis. When the specimen was loaded under 0.2 kN and submitted to an external vibration excitation, no influence on the shape of the Lamb

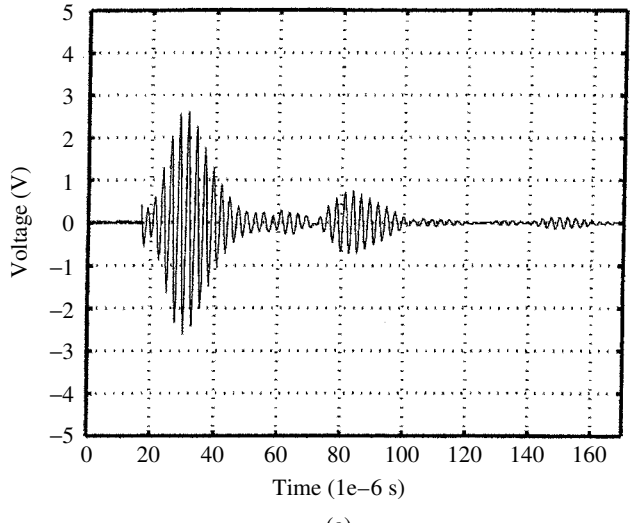

(a)

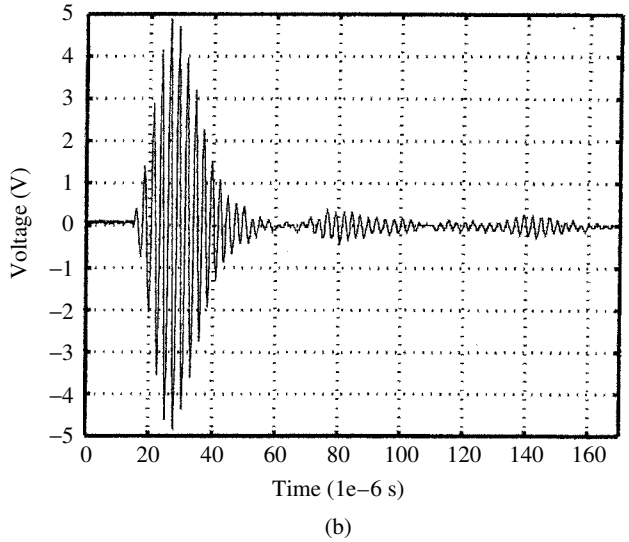

(b)

Figure 4.37 Lamb wave responses from sensor R1: (a) undamaged plate; (b) damaged plate

wave signal was observed, which proves that loading did not have any influence regarding the signal recorded. However, after a damaging impact at location 4, one of the modes is lost, as shown in Figure 4.37b. The presence of delamination was confirmed using a conventional ultrasonic A-scan. Figure 4.38 gives the local minima of the envelope function calculated using the Hilbert transform (Randall 1987). These minima, corresponding to mode changes due to damage, can be used for damage detection.

Figure 4.39 shows the time history of the Lamb wave response for the transmission test between the E2 and R2 transducers before the impact tests were performed (*no damage* condition). The signal exhibits more complex modes because of the geometry of the analysed plate (thickness variations and stiffener). Further testing reveals a clear

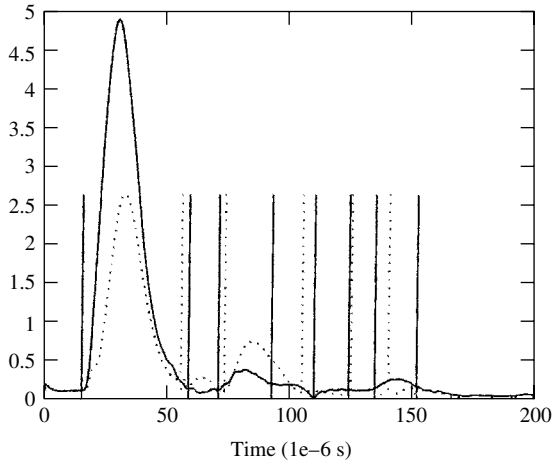

Figure 4.38 Local minima for the Lamb wave responses from sensor R1: dashed line – before testing, solid line – after damaging impact

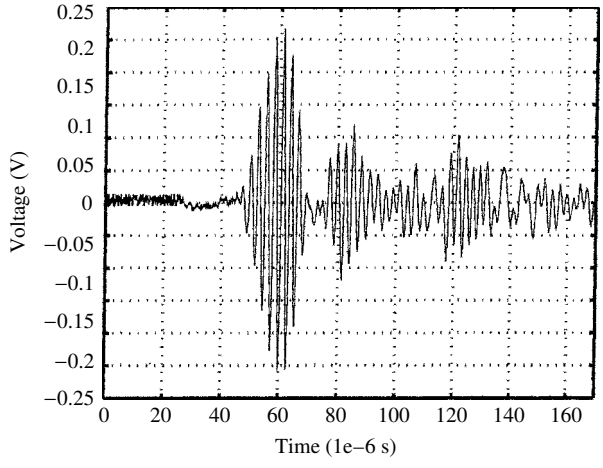

Figure 4.39 Lamb wave responses from sensor R2 for the undamaged plate

delamination in the composite plate due to the damaging impact at location 3, as shown in Figure 4.40.

Finally, the composite plate was submitted to cyclic loading. An example of local minima for the Lamb wave responses is presented in Figure 4.41. The result displays phase delays and mode conversions due to the growth (by 1 cm) of the disbond.

These simple experimental tests demonstrate the ability of the Lamb wave testing method to detect and monitor various types of defects in composite materials. The technology is capable to perform continuous, in-service health and usage monitoring of aircraft structures. Further examples are shown in Chapter 6.

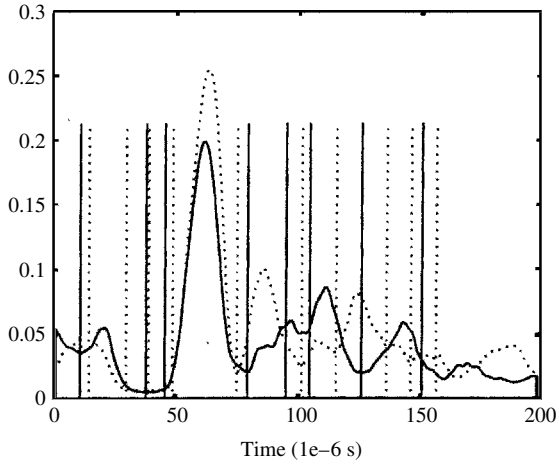

Figure 4.40 Local minima for the Lamb wave responses from sensor R2 dashed line – before testing (dashed line) and after damaging impact (solid line)

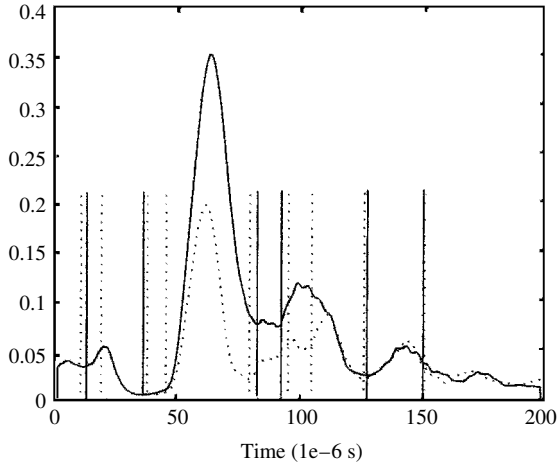

Figure 4.41 Local minima for the Lamb wave responses after damaging impact (dashed line) and after cycling loading (solid line)

4.9 SUMMARY

A brief introduction to damage detection methods based on sound and ultrasound has been given in this chapter. The presentation includes AE, Ultrasonics, Acousto-Ultrasonics and guided wave Ultrasonics. The material presented shows that there are various similarities between these techniques. All these techniques utilise piezoceramic transducers for damage monitoring and testing. Therefore a brief description of piezoceramic materials has been given for the sake of completeness. Simple application examples show how the methods work in practice. The potential of the methods for aerospace applications is presented in Chapter 6 where various large-scale and flight test examples are given.

REFERENCES

Acellent Technologies, web page: **www.acellent.com**

Achenbach, J.D. 1984. *Wave Propagation in Elastic Solids*, North–Holland, New York.

Agostini, V., Delsanto, P.P. and Zoccolan, D. 2000. Flaw detection in composite plates by means of Lamb waves, *Proceedings of the 15th World Conference on NDT*, Roma, Italy, 15–21 October.

Assaad, J., Bruneel, C., Decarpigny, J.N. and Nongaillard, B. 1990. The finite element code at ISEN (IEMN), Proceedings of the workshop held in Toulon, France, June 1990.

Betz, D., Thursby, G., Culshaw, B. and Staszewski, W.J. 2002. Acousto-ultrasonic sensing using fiber Bragg gratings, *Smart Materials and Structures*, Vol. 12, No. 1, pp. 122–128.

Biemans, C., Staszewski, W.J., Boller, C. and Tomlinson, G.R. 2001. Crack detection in metallic structures using broadband excitation of acousto-ultrasonics, *Journal of Intelligent Materials Systems and Structures*, Vol. 12, No. 8, pp. 589–597.

Buirks, A.S., Green Jr, R.E. and McIntyre, P. (eds). 1991. *Nondestructive Testing Handbook*, Vol. 7, *Ultrasonic testing*, American Society of Nondestructive Testing, Columbus, Ohio.

Chang, F.K. 1998. Smart layer built-in diagnostics for composite structures, *Proceedings of the 4th European Conference on Smart Materials and Structures and the 2nd MIMR Conference*, Harrogate, UK, 6–8 July, pp. 777–781.

Delsanto, P.P., Whitcombe, T., Chaskelis, H.H. and Mignogna, R.B. 1992. Connection machine simulation of ultrasonic wave propagation in materials – I: the one-dimensional case, *Wave Motion*, Vol. 16, pp. 65–80.

Delsanto, P.P., Schechter, R.S., Chaskelis, H.H., Mignogna, R.B. and Kline, R.B. 1994. *Connection machine simulation of ultrasonic wave propagation in materials – II: The two-dimensional case*, Vol. 20, pp. 295–314.

Delsanto, P.P., Schechter, R.S., and Mignogna, R.B. 1997. *Connection machine simulation of ultrasonic wave propagation in materials – III: The three-dimensional case*, Vol. 26, pp. 329–339.

Egusa, S. and Iwasawa, N. 1993. Polling characteristics of PZT/epoxy piezoelectric paints, *Ferroelectrics*, Vol. 145, pp. 45–60.

Envirocoustics S.A. web page: **www.pacndt.com**

Holroyd, T. 2001. *The Acoustic Emission and Ultrasonic Monitoring Handbook*, Coxmoor Publishing Company, Oxford, UK.

Khuri-Yakub, B.T., Cheng, C.H., Degertekin, F.L., Ergun, S., Hansen, S., Jin, X.C. and Orlakan, O. 2000. Silicon micromachined ultrasonic transducers, *Japanese Journal of Applied Physics*, Vol. 39, pp. 2882–2887.

Kiernanand, M.T. and Duke Jr, J.C. 1988. PC analysis of an acousto-ultrasonic signal, *Materials Evaluation*, Vol. 46, No. 9, pp. 1344–1352.

Kwon, O.Y., Kim, T.H. and Lee, K.J. 2000. Monitoring fatigue damage in adhesively bonded composite–metal joints by acoustic methods, *Proceedings of the 15th World Congress on NDT*, Roma, Italy, 15–21 October.

Lee, B.C. and Staszewski, W.J. 2002. Modeling of acousto-ultrasonic wave interactions with defects in metallic structures, *Proceedings of the International Conference on Noise and Vibration Engineering – ISMA* 2002, Leuven, Belgium, 16–18 September.

Lee, B.C. and Staszewski, W.J. 2003a. Lamb wave interactions with structural defects – modelling and simulations, *Proceedings of the SPIE's 10th International Symposium on Smart Structures and Materials, Conference on Modeling, Signal Processing and Control*, San Diego, California, 2–6 March, Paper No. 5049-22.

Lee, B.C. and Staszewski, W.J. 2003b. Modelling of Lamb waves for damage detection in metallic structures, Part I: wave propagation, *Smart Materials and Structures*, Vol. 12(5), pp. 804–814.

Lee, B.C. and Staszewski, W.J. 2003c. Modelling of Lamb waves for damage detection in metallic structures, Part II: wave interactions with damage, *Smart Materials and Structures*, Vol. 12(5), pp. 815–824.

Moulin, E., Assaad, J., Delebarre, C., Kaczmarek, H. and Balageas, D. 1997. Piezoelectric transducer embedded in a composite plate: application to Lamb wave generation, *Journal of Physics*, Vol. 82, No. 5, pp. 2049–2055.

Muravin, G. 2000. *Inspection, Diagnostics and Monitoring of Construction Materials and Structures by the Acoustic Emission Methods*, Minerva Press, London, UK.

Pedemonte, P., Staszewski, W.J., Aymerich, F., Found, M.S. and Priolo, P. 2001. Signal processing for passive impact damage detection in composite structures, *Proceedings of the SPIE's 8th International Symposium on Smart Structures and Materials, Conference on Modeling, Signal Processing and Control, Newport Beach*, California, 4–8 March, Paper No. 4326-19.

Randall, R.B. 1987. *Frequency Analysis*, 3rd edition, Brüel & Kjæl Publications, Nærum, Denmark.

Rose, J.L. 1999. *Ultrasonic Waves in Solid Media*, Cambridge University Press, Cambridge, UK.

Schmerr Jr, L.W. 1998. *Fundamentals of Ultrasonic Nondestructive Evaluation: A Modeling Approach*, Plenum Publishing Corporation, New York.

Scott, I.G. 1991. *Basic Acoustic Emission*, Gordon and Breach Science Publishers, New York, NY.

Staszewski, W.J. and Boller, C. 2002. Acoustic wave propagation phenomena modelling and damage mechanisms in ageing aircraft, *Proceedings of the Aircraft Integrated Monitoring Systems Conference – AIMS, Garmisch-Partenkirchen*, Germany, 27–30 May, pp. 169–184.

Staszewski, W.J. and Holford, K. 2001. Wavelet signal processing for acoustic emission data, *Proceedings of the 4th International Workshop on Damage Assessment Using Signal Processing Procedures – DAMAS-2001*, Cardiff, Wales, 25–27 June.

Staszewski, W.J., Biemans, C., Boller, C. and Tomlinson, G.R. 1999a. Crack propagation monitoring in metallic structures, *Proceedings of the International Conference on Smart Materials, Structures*, Bangalore, India, 7–10 July, pp. 532–541.

Staszewski, W.J., Biemans, C., Boller, C. and Tomlinson, G.R. 1999b. Impact damage detection in composite structures, *Proceedings of the 2nd International Workshop on Structural Health Monitoring*, Stanford, California, 8–10 September, pp. 754–763.

Vary, A. 1988. The acousto-ultrasonic approach. In: J.C. Duke Jr (ed.), *Acousto-Ultrasonics: Theory and Application*, Plenum Press, New York, pp. 1–21.

Viktorov, I.A. 1967. *Rayleigh and Lamb Waves*, Plenum Press, New York.

Wilcox, P.D., Dalton, R.P., Lowe, M.J.S. and Cawley, P. 1999. Mode transducer selection for long range Lamb wave inspection, *Proceedings of the 3rd International Workshop on Damage Assessment Using Advanced Signal Processing – DAMAS* 1999, Dublin, Ireland, 28–30 June, pp. 152–161.

Yoshikawa, S. Selvaraj, U., Moses, P., Witham, J., Meyer Jr, R. and Shrout, T. $Pb(Zr,Ti)O_3$ [PZT] fibers – fabrication and measurement methods, *Journal Intelligent Materials, Systems and Structures*, Vol. 6, pp. 152–158.